Local and Global Paratropic and Diatropic Ring Currents in Pyrene and Its Cyclopenta-Fused Congeners

Erich Steiner,[a] Patrick W. Fowler,[a] Leonardus W. Jenneskens,*[b] and Remco W. A. Havenith[a]

Keywords: Ab initio calculations / Anti-aromaticity / Aromaticity / NMR spectroscopy

An ab initio distributed-origin coupled Hartree–Fock method has been used to compute the σ-, π- and total (σ+π)-current density maps of a family of polycyclic aromatic hydrocarbons comprising pyrene (**1**) and its externally cyclopenta-fused congeners **2**–**8**. The number and the distribution of pentagons strongly affect the local patterns of induced currents, and global aromaticity is reduced as more pentagons are added to the pyrene perimeter. The pentagons in **2** and **3** have only minor effects on the pyrene core and contain cyclopenteno double bonds. In the case of the other species **4**–**8**, in marked contrast, intense paratropic currents in the pentagons result in stepwise destruction of the 14π pyrene perimeter motif and the breaking up of the currents into single-ring contributions. The visualisation adds detail to the interpretation of Nucleus-Independent Chemical Shift (NICS) values, and the pattern of paratropic contributions can in fact, with the exception of **6** and **7**, be explained qualitatively by simple Hückel–London π-electron theory.

Introduction

Although ring currents are not directly observable, their existence has been inferred from magnetic measurements such as ^{1}H NMR chemical shifts [$\delta(^1H)$], magnetic anisotropy ($\Delta\xi$) and exaltation of isotropic magnetic susceptibility (Λ).[1] These properties, which are determined by integration of the induced current density, are of considerable practical and theoretical interest. They are intimately linked with the concept of (anti-)aromaticity − the ability to sustain (para-) diatropic ring currents. In the case, however, of π-conjugated polycyclic compounds consisting of a mixture of annulated odd- and even-membered rings, interpretation of the *global*, molecular magnetic properties in terms of *local* diatropic and paratropic contributions of distinct rings is not always straightforward.[2]

Some years ago, Schleyer and co-workers introduced the *isotropic* Nucleus-Independent Chemical Shift (NICS) technique as a probe for these local ring-current contributions.[3] The mean absolute nuclear shielding (σ_{av}) in the geometric centre of a ring is computed and converted into a shift by reversing its sign. A negative sign thus reflects local diatropic ring current contributions, whilst a positive sign indicates local paratropic ring current contributions. The strength of the NICS criterion is that it reduces the characterisation of a ring to the evaluation of a single numerical quantity, although this simplicity can also be a weakness in that a single number may mask cancellation or anisotropy between contributions. Several expedients can be envisaged: NICS can be decomposed into *in-plane* and *out-of-plane* tensor components,[4] or can be computed at various out-of-plane positions and its dependence on the distance from the ring centre taken to reflect the balance of local in- and out-of-plane components.[5]

A different approach, which provides information at a finer level of detail, is by visualisation and analysis of the all-electron [σ-, π-, and total (σ+π)-] current density maps themselves. Direct computation and inspection of these maps allows diatropicity and paratropicity to be assessed on global (molecular) and local (ring and bond) scales. Ab initio all-electron distributed-origin methods using continuous transformation of origin of current density (CTOCD)[6] have been successfully applied to several conjugated π-system families.[7,8] The reliability of the computed maps is demonstrated by the agreement of the integrated properties with experimental data.

The maps also give new insights that contribute to long-standing chemical debates. For example, the "annulene-within-an-annulene" model[9] for corannulene and coronene[8a] and for kekulene[8b] can now be decisively rejected on the basis of all-electron distributed-origin calculations, which show counterrotating rim and hub currents, in

[a] School of Chemistry, University of Exeter,
Stocker Road, Exeter EX4 4QD, U.K.
[b] Debye Institute, Department of Physical Organic Chemistry, Utrecht University,
Padualaan 8, 3584 CH Utrecht, The Netherlands
Fax: (internat.) + 31-30/253-4533,
E-mail: jennesk@chem.uu.nl
[c] Debye Institute, Theoretical Chemistry Group, Utrecht University,
Padualaan 8, 3584 CH Utrecht, The Netherlands

  1434−193X/02/0101−0163 $ 17.50+.50/0

contrast to the conrotating diatropic circulations expected from the annulene model.

In this paper we report and discuss the computed current density maps of a family of polycyclic aromatic hydrocarbons (PAH) comprising pyrene (**1**) and its known cyclopenta-fused congeners cyclopenta[*cd*]pyrene (**2**),[10] the isomeric dicyclopenta[*cd*,*mn*]- (**3**), dicyclopenta[*cd*,*jk*]- (**4**) and dicyclopenta[*cd*,*fg*]pyrene (**5**),[11] tricyclopenta[*cd*,*fg*,*mn*]pyrene (**6**)[12] and the elusive tetracyclopenta[*cd*,*fg*,*jk*,*mn*]pyrene (**7/8**,[13] see Computational Section) (Scheme 1).

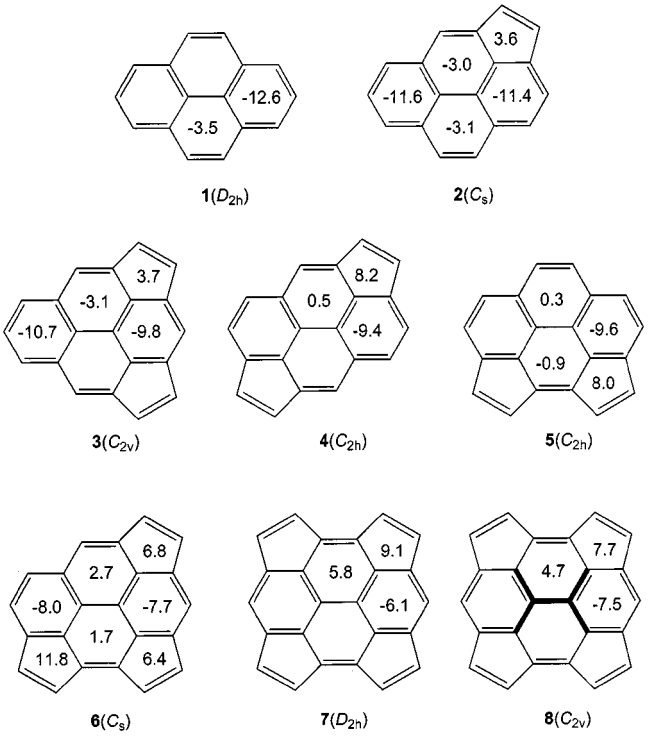

Scheme 1. Molecules under study; the values reported in the distinct rings IGLO-III//RHF/6-31G NICS (0.0 Å) are taken from ref.[19]

This family is not without its chemical and physical features of interest. Compounds **1**−**5** are abundant combustion effluents, and the cyclopenta-fused congeners **2**−**5** pose a potential biohazard because of their genotoxic properties.[14] In addition, **1**−**8** represent topological substructures of the fullerenes.[15] Furthermore, the nonalternant character of **2**−**8** can produce unusual physicochemical properties such as high electron affinities[13] and characteristic upfield-shifted ^{1}H NMR chemical shifts,[2,11,12] together with photophysical properties such as UV/Vis spectra that are strongly modulated by the number and distribution of cyclopenta moieties,[11,12] and anomalous fluorescence.[16]

In the case of **1**−**6**, experimental and theoretical evidence indicates that the cyclopenta moieties have marked effects on the global aromaticity. The average ^{1}H NMR chemical shift values of the six- and the five-membered ring protons [$\delta(6)_{av}$ = 8.14 (**1**)[17] and $\delta(6)_{av}/\delta(5)_{av}$: 8.18/7.32 (**2**),[10] 8.32/7.36 (**3**),[11] 7.55/6.66 (**4**),[11] 7.58/6.90 (**5**)[11] and 7.44/6.74 (**6**)[12]] show that, in comparison with **1**−**3**, **4**−**6** possess reduced aromatic character. These observations are supported by computation of the integrated global magnetic properties of **1**−**8** (χ_{tot}, Λ, ^{1}H NMR chemical shifts) at the ab initio GIAO and IGLO-III levels of theory,[18] in which the reduced global aromatic character of **4**−**6** is indicated by falling computed χ_{tot} and Λ values, despite the simultaneous increase in size of the conjugated π-systems. The computed NICS values for the distinct six- and five-membered rings in **1**−**8** (Scheme 1) also indicate that the *global* effects are accompanied by significant *local* changes (see also refs.[18,19]); it is these changes in local magnetic response that are explored in detail in the present calculations.

Results and Discussion

σ-, π- and Total (σ+π)-Current Density Maps

For the planar molecules **1**−**7** the current densities induced by a unit magnetic field perpendicular to the molecular plane are shown in Figures 1−3. In a field pointing out of the page, an induced anticlockwise circulation of electrons is diamagnetic whilst a paramagnetic circulation is clockwise. The current densities were computed in a plane parallel to and at a distance of 1 a_0 (1 a_0 = 0.5292 Å) from

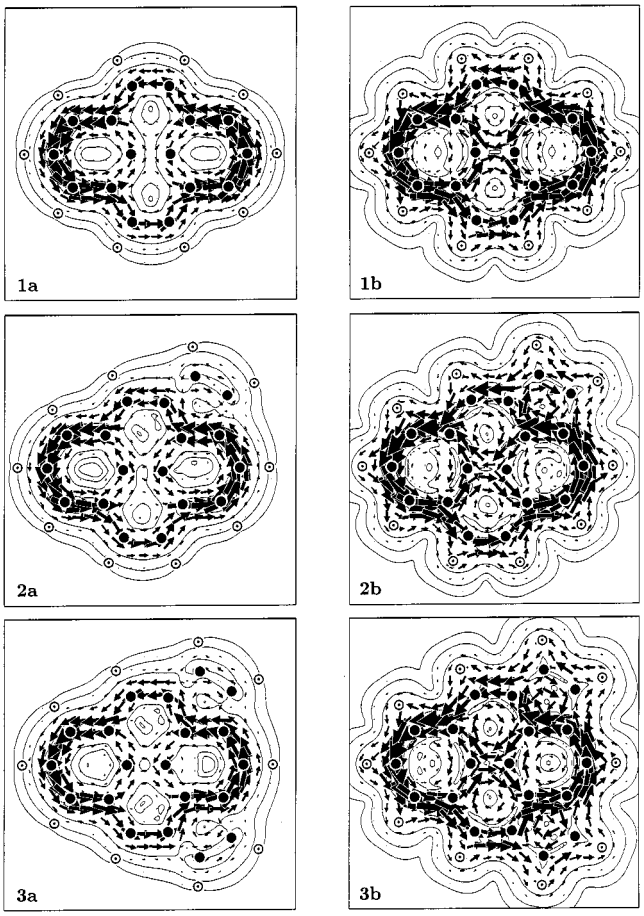

Figure 1. Computed CTOCD current density maps for **1**−**3**: (a) π and (b) total (σ+π) (● carbon, ⊙ hydrogen; nuclear positions projected in the plotting plane)

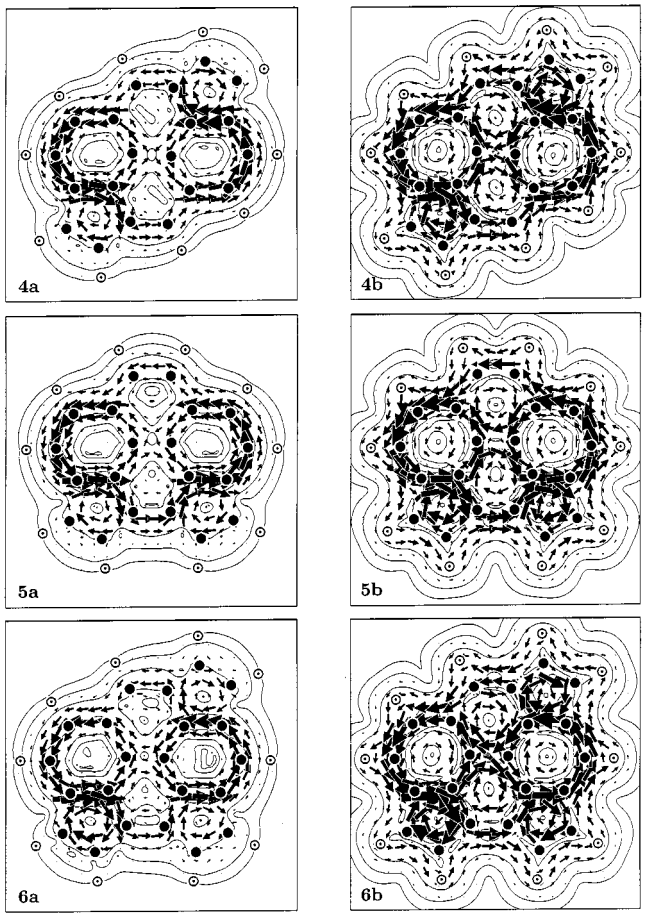

Figure 2. Computed CTOCD current density maps for **4**−**6**: (a) π and (b) total (σ+π) (● carbon, ⊙ hydrogen; nuclear positions projected in the plotting plane)

the plane of the nuclei, chosen so as to lie close to the maxima of both π-current and π-electron density. At this height the flow is essentially parallel to the molecular plane. The plotting area is a square of side 24 a_0. The contours show the modulus of the complete current density, with values 0.001×4^n a.u., for $n = 0,1,2, \ldots$ The vector arrows are centred on points of a 36 × 36 grid, and show the magnitude and the direction of the in-plane projection of current. The current-density maps shown are for (a) π- and (b) total (σ+π)-electron distributions in the chosen plane.

At this distance from the molecular plane, the details of the σ-current density near the nuclei are lost, but σ-maps generally demonstrate distributions of current that are characteristic of covalent bonds,[7a] in which each σ-bond acts as a centre of local diamagnetic circulation. The cumulative effect of these local circulations in each ring is a characteristic paramagnetic σ-circulation over the centre of the ring, which can be seen here in the total (σ+π)-maps.

Map 1a in Figure 1 shows the π-current density distribution in the parent compound pyrene (**1**). Its most striking feature is a classical diatropic circulation around the 14π-pyrene perimeter, which subsumes local benzene-like currents in the two hexagons (*A* and *B*) of the biphenyl-like subunit. In the central rings *C* and *D*, some bifurcated flow

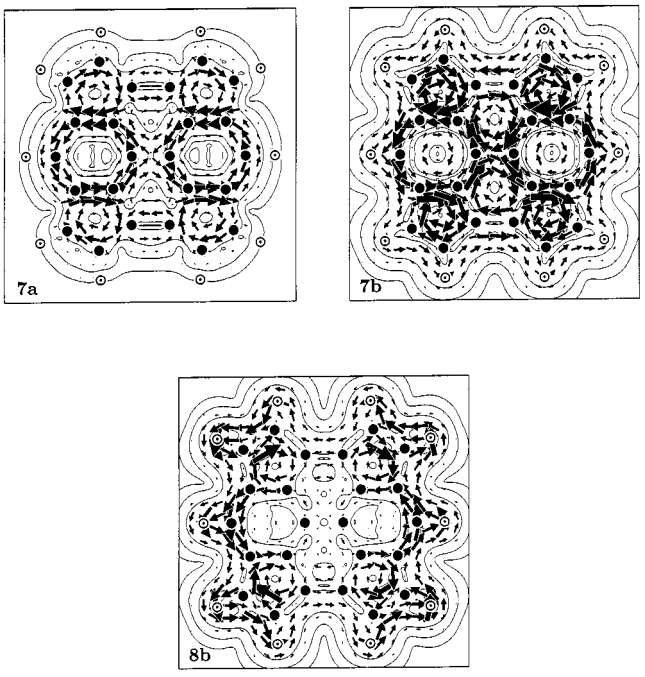

Figure 3. Computed CTOCD current density maps for **7**: (a) π and (b) total (σ+π), and for **8**: (b) total (σ+π; the plotting plane is 0.85 a_0 above the median plane, see text); in all maps: ● carbon, ⊙ hydrogen; nuclear positions projected in the plotting plane

of the ring current is discernible in the π-map.[18,20] These features are present in an accentuated form in the total (σ+π)-current density map (map 1b, Figure 1).

Fusion of a single cyclopenta moiety onto **1** to give **2** produces no essential change in the circulations within the pyrene subunit [π- and total (σ+π)-maps, **2a** and **2b**, Figure 1 and Scheme 1]. The added pentagon *E* contains a localised cyclopenteno double bond, which makes little contribution to the π-currents;[19] the pentagonal ring also supports the usual weak central σ paramagnetic current that arises from local bond currents.

Fusion of a second cyclopenta moiety to **2** gives three isomeric possibilities: compounds **3**−**5** (Schemes 1 and 2). When the pentagons are positioned as in **3** (*E* and *F*) − that is, when they are separated by two carbon−carbon bonds − they again contain localised double bonds and cause little perturbation to the diatropic 14π-pyrene perimeter ring current [π- and total (σ+π)-maps, 3a and 3b, Figure 1].

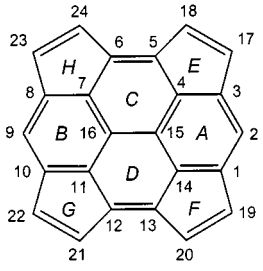

Scheme 2. Generalised carbon atom numbering and local ring identification Scheme for pyrene (**1**) and its cyclopenta-fused congeners **2**−**8**

In marked contrast, the isomers **4** and **5**, in which the pentagon pairs are linked by an odd number of carbon−carbon bonds (**4**: *E* and *G*, three bonds; **5**: *F* and *G*, one bond; Scheme 1), show new features [π- and total (σ+π)-maps, **4a** to **5b**, Figure 2 and Scheme 2]. The pentagons now exhibit *para*magnetic π-ring currents, which are reinforced by the central σ-circulations in the total (σ+π)-current maps. As a consequence, the total (σ+π)-current maps for **4** and **5** no longer show a clearly separated pyrene-perimeter motif. The main features are the local benzene-like currents in the hexagons *A* and *B*, and the paratropic currents in the five-membered rings.

At the next stage, in which a third pentagon *G* is added to give the unique pyrene congener with three cyclopenta moieties **6** (*E*, *F* and *G*), the weakening of the 14π-pyrene perimeter pattern proceeds a step further (Schemes 1 and 2). Although the π-distribution still shows the two original diamagnetic hexagons *A* and *B*, three paramagnetic pentagons *E*, *F* and *G*, of which ring *G* is connected by an odd number of carbon−carbon bonds to both of the other pentagons, carry a significantly stronger paramagnetic ring current (Scheme 2). Moreover, the original diatropic pyrene perimeter current is now attenuated by incipient localisation in the C(5)−C(6) [C(12)−C(13)] bond [π- and total (σ+π)-maps 6a and 6b, Figure 2].

Addition of a fourth pentagon gives the as yet unsynthesised tetracyclopenta[*cd*,*fg*,*jk*,*mn*]pyrene (**8**; Scheme 1). Calculations[18,19] indicate that **8** should have a bowl-shaped ground-state structure [RHF/6-31G; **8** (C_{2v}): bowl depth ca. 0.90 Å, similar to that in corannulene[8a,21]] in which a rigid σ/π separation can no longer be applied. We therefore start with an analysis of its planar analogue **7** (D_{2h}), which represents the transition state for bowl-to-bowl interconversion [RHF/6-31G: $\Delta E(\mathbf{8} \rightarrow \mathbf{7})$ = 3.8 kcal mol^{-1}; see Computational Section and Scheme 1]. The π-current map of **7** shows that, upon addition of the fourth pentagon, the breaking up of the 14π-pyrene perimeter motif is completed. The π-current map splits into two halves in which the diamagnetic ring currents of the biphenyl-like hexagons *A* and *B* survive unscathed between two strongly paramagnetic circulations in the neighbouring pentagons *E*−*H* [π- and total (σ+π)-maps 7a and 7b, Figure 3 and Scheme 2]. These qualitative features are reinforced in the total (σ+π)-map of planar **7**. As a curved structure, **8** no longer supports a rigid σ/π-separation, and the concept of a near-planar ring current is not appropriate. Nevertheless, the total (σ+π)-map for the bowl (map 8b, Figure 3; plotting plane at 0.85 a_0 above the median plane, "looking into the bowl") still shows all the features of planar **7**: the paramagnetic circulations in the pentagons, diamagnetic circulations in the (now more distant) hexagons and the destruction of the pyrene-perimeter motif.

Comparison with Nucleus-Independent Chemical Shifts

Scheme 1 shows the NICS (0.0 Å) values for all distinct local rings of **1**−**8**; the values are derived from IGLO-III//RHF/6-31G calculations at the ring centres.[19] Comparison of these values with the local patterns of current in the maps of Figures 1 and 3 shows complete qualitative agreement. The local diamagnetic ring currents of the maps correspond to large negative NICS values in rings *A* and *B* of all the structures. The hexagons *C* and *D*, which display bifurcated flows in the maps, have small NICS values, which may be of either sign in particular cases. The pentagons *E*−*H* change from having small positive NICS values for those cases in which the maps show that the cyclopenteno double bonds are localised (**2**, **3**) to large positive NICS values in **4**−**7**, in which the maps show significant paramagnetic currents for these rings. The maps therefore provide a direct visualisation of the changing patterns of induced current density that underlie the original NICS analysis,[3] but they are also capable of supplying more detail than the bare average NICS values.

Table 1 lists the nuclear shieldings (σ) for all distinct ring centres in **1**−**8**, obtained by the appropriate integration of the CTOCD-PZ2 current densities. The averages σ_{av} are equivalent to NICS values, apart from the change of sign in the definition.[7,8] With allowance for basis set and method differences, they are essentially in agreement with those

Table 1. Computed nuclear shielding constants at the ring centres of **1**−**8** (in ppm); σ(out) is the component of the *out-of-plane* nuclear shielding constants of the ring, σ(in) is the mean shielding *in-plane*, and σ_{av} the overall mean value

Compound[a]	Ring[a]	σ(out)	σ(in)	σ_{av} [a]
1	*A*	23.7	12.5	16.2
	C	−3.7	15.2	8.9
2	*A*	18.7	15.3	16.4
	B	20.8	12.3	15.1
	C	−6.1	13.9	7.2
	D	−4.7	14.6	8.1
	E	−35.9	13.1	−3.2
3	*A*	12.7	13.5	13.2
	B	16.1	13.9	15.3
	C	−6.1	13.8	7.2
	E	−36.1	12.9	−3.4
4	*A*	13.3	15.6	14.8
	C	−15.2	13.9	4.2
	E	−48.2	13.0	−7.4
5	*A*	13.8	15.4	14.8
	C	−14.3	14.3	4.8
	D	−14.4	14.7	5.0
	F	−48.1	12.4	−7.7
6	*A*	7.3	13.9	11.7
	B	9.4	15.1	13.2
	C	−22.0	13.8	1.9
	D	−20.8	14.2	2.5
	E	−44.0	13.1	−6.0
	F	−43.2	12.6	−6.0
	G	−57.8	12.3	−11.1
7	*A*	3.1	13.8	10.2
	C	−32.5	14.2	−1.4
	E	−49.8	12.4	−8.3
8[b]	*A*	−	−	10.7
	C	−	−	−0.6
	E	−	−	−7.8

[a] See Scheme 2. For a comparison of σ_{av} values with IGLO-III//RHF/6-31G NICS(0.0 Å) values[19] see Scheme 1. [b] For bowl-shaped **8** only σ_{av} was calculated.

shown in Scheme 1. Whereas for the hexagons *A*−*D* the σ_{av} values are similar for **1**−**2**, they become less positive on going from **3** to **8**, upon addition of an increasing number of (abutting) pentagons. For the pentagons *E*−*H* the opposite behaviour is found. Their small negative σ_{av}-values, which are only slightly negative in the case of **2**−**3**, become considerably more negative for **4**−**8**.

Decomposition of these σ_{av} values into *out-of-plane* [σ(out)] and average *in-plane* [σ(in)] components gives more information. It can be seen that the out-of-plane component is sensitive to changes in the ring currents of the distinct rings of these polycyclic π-conjugated systems. The σ(out) component picks out the jumps in pentagon paramagnetism between **2**, **3** and **4**, **5**, and distinguishes the two types of pentagons in **6**. The σ(in) component, on the other hand, is relatively constant, so that the averaging over three components inherent in the NICS computation results in some loss of sensitivity.

Magnetisability Anisotropy Δξ and Nuclear Chemical Shifts

Magnetisability anisotropy [Δξ= ξ(out) − ξ(in)], computed by integration of the CTOCD-PZ2 current density, is one indicator of global aromaticity. The Δξ values obtained by the present approach are −55.9 (**1**), −59.3 (**2**), −62.5 (**3**), −51.0 (**4**), −52.1 (**5**), −48.0 (**6**), −39.0 (**7**) a.u. ($e^2a_0^2/m_e$), and can be interpreted as indicative of similar global aromaticities in **1**−**3**, with a fall-off in **4**−**8** as the proportion of local paramagnetism increases (Table 2). Decomposition of ξ_{av} into out-of-plane [ξ(out)] and average in-plane [ξ(in)] components shows that the changes of Δξ stem from considerable changes in ξ(out), whilst ξ(in) changes only moderately in line with the increase in size of the π-system. In view of the known correlation of calculated magnetisability anisotropy (Δξ) with empirical *isotropic* exaltation of diamagnetic susceptibility (Λ),[8a] this suggests a concomitant fall in *Λ* along the series. By the same computational approach, the anisotropies Δξ (a.u.) = −16.5 (benzene), −30.5 (naphthalene), −45.1 (fluoranthene), −55.9 [pyrene (**1**)] can be compared with the diamagnetic exaltations Λ (10^{-6} cm^3 mol^{-1}) = 13.7, 30.5, 42, 57, respectively.[1c]

Table 2. Computed molecular magnetisabilities of **1**−**8** (in a.u.)[a]; ξ(out) is the component of the absolute *out-of-plane* shielding of the molecule, ξ(in) is the mean *in-plane* shielding, ξ_{av} the overall mean value, and Δξ = ξ(out) − ξ(in) is the anisotropy

Compound	ξ(out)	ξ(in)	ξ_{av}	Δξ
1	−67.6	−11.7	−30.4	−55.9[b]
2	−71.9	−12.6	−32.4	−59.3
3	−76.1	−13.6	−34.4	−62.5
4	−64.7	−13.7	−30.7	−51.0
5	−65.9	−13.8	−31.2	−52.1
6	−62.5	−14.5	−30.5	−48.0
7	−54.6	−15.6	−28.6	−39.0
8[c]	–	–	−30.6	–

[a] Magnetisabilities are given in atomic units: 1 a.u. = $e^2a_0^2/m_e$ = 7.89104 × 10^{-29} J T^{-2}. [b] *Isotropic* exaltation of diamagnetic susceptibility of **1** 57 × 10^{-6} cm^3 mol^{-1} (see text).[1c,8a] Unfortunately, no Λ values are available for **2**−**8**. [c] For bowl-shaped **8** only ξ_{av} was calculated.

The changes in local environment shown in the series of maps (Figures 1−3) have their counterparts in the computed nuclear chemical shifts. The calculated CTOCD-PZ2 ^{1}H NMR chemical shifts (Table 3) are generally shifted upfield by up to 0.6 ppm from the corresponding available experimental values, but the general features and trends found experimentally for **1**−**6** both within a compound and between related compounds are qualitatively reproduced. For example, the ^{1}H NMR chemical shift of H(2), connected to hexagon *A* and positioned *exo* to the pentagons (Scheme 2), reflects the steady increase in paratropicity throughout the series, from δ = 8.0 in **1** to δ = 6.0 in **8** (Table 3). Other indicators such as the computed ring-averaged ^{1}H NMR chemical shifts of the six- and five-membered rings [$\delta(6)_{av}/\delta(5)_{av}$] produce the same conclusion [exp. (calcd.): $\delta(6)_{av}$ = 8.14 (7.8) (**1**); $\delta(6)_{av}/\delta(5)_{av}$ = 8.18/7.32[10] (7.8/7.1) (**2**), 8.32/7.36[11] (7.9/7.2) (**3**), 7.55/6.66[11] (7.4/6.7) (**4**), 7.58/6.90[11] (7.4/6.8) (**5**), 7.44/6.74[12] (7.1/6.6) (**6**)]. Interestingly, for the as yet unsynthesized bowl-shaped congener **8**, CTOCD-PZ2 predicts the most strongly upfield-shifted δ(^{1}H) values, in line with the total (σ+π)-map (map 8b, Figure 3 and Table 3).

Hückel−London π-Electron plots

The ab initio results show dominance by paramagnetic pentagons in the current densities in **4**−**8**. Could these currents have been expected on the basis of an intuitive chemical model? One simple approach is to use Hückel π-electron theory in conjunction with the London model.[22−24] Sets of π-bond currents computed according to a finite-perturbation, matrix-diagonalisation procedure for planar **1**−**7** are shown in Figure 4. The calculations used the 6-31G ab initio geometries scaled to an average bond length of 1.4 Å for calibration against a notional benzene π-bond current. It is impressive that these simple idealisations exhibit all the main features of the ab initio maps in most cases, even if they exaggerate the relative strength of the paratropic currents and thus, in the case of **6** and **7,** give a qualitatively incorrect picture. Nonetheless, at this Hückel−London level of theory the importance of the paratropic pentagon as a motor for the total pattern is apparent from this purely graph-based theoretical model.

Magnetic versus Energy Criteria for Aromaticity; Isomers **3**−**5**

Despite the increase in area of the π-electron system with increasing number of pentagons in series **1**−**8**, the fall in CTOCD-PZ2 Δξ values (Table 2), which was also found when using either GIAO or IGLOIII,[18,19] shows that the global aromatic character decreases throughout the whole series. For isomers **3**−**5**, a comparison of their relative stabilities [ΔE_{tot}(**5** < **4** < **3**) = 0.0 < 1.9 < 4.3 kcal mol^{-1}, see Computational Section] and their computed |Δξ| values [**3** > **5** > **4**: 62.5 > 52.1 > 51.0 a.u.; Table 2] indicates that **3**−**5** possess a different order of aromaticity according to

Table 3. Computed absolute hydrogen nuclear shielding constants (in ppm) of **1**−**8**; σ(out) is the component of the *out-of-plane* hydrogen nuclear shielding constants of the ring, σ(in) is the mean *in-plane* shielding, and σ_{av} the overall mean value; the corresponding δ values (in ppm) were obtained by using $\delta = 30.8 - \sigma_{av} \times 10^6$ [8a,8b]

Compound	Nucleus[a]	σ(out)	σ(in)	σ_{av}	$\delta_{calcd.}$	δ_{exp}
1	H(2)	18.2	25.1	22.8	8.0	8.0
	H(3)	17.1	25.8	22.9	7.9	8.2
	H(5)	17.6	26.0	23.2	7.6	8.1
2	H(1)	16.9	25.8	22.9	7.9	8.1
	H(2)	17.5	25.7	23.0	7.8	8.1
	H(6)	16.8	26.3	23.1	7.7	8.4
	H(8)	17.0	25.5	22.7	8.1	8.4
	H(9)	18.2	25.1	22.8	8.0	8.0
	H(10)	17.4	25.6	22.9	7.9	8.3
	H(12)	17.9	25.9	23.2	7.6	8.1
	H(13)	17.7	25.8	23.1	7.7	8.0
	H(17)	20.9	25.0	23.6	7.2	7.4
	H(18)	21.0	25.2	23.8	7.0	7.2
3	H(2)	17.0	26.3	23.2	7.6	8.1
	H(6)	16.9	26.2	23.1	7.7	8.3
	H(8)	17.2	25.3	22.6	8.2	8.4
	H(9)	18.2	25.1	22.8	8.0	8.0
	H(17)	20.7	24.8	23.5	7.3	7.5
	H(18)	21.0	25.2	23.8	7.0	7.2
4	H(1)	18.3	25.5	23.1	7.7	7.7
	H(2)	18.9	25.7	23.5	7.3	7.4
	H(13)	18.8	26.2	23.7	7.1	7.5
	H(17)	22.4	25.0	24.1	6.7	6.6
	H(18)	22.6	25.0	24.2	6.6	6.7
5	H(1)	18.4	25.6	23.2	7.6	7.7
	H(2)	18.8	25.7	23.4	7.4	7.6
	H(13)	19.3	25.8	23.6	7.2	7.4
	H(17)	22.0	24.9	23.9	6.9	7.0
	H(18)	21.7	25.4	24.2	6.6	6.8
6	H(2)	19.1	26.3	23.9	6.9	7.4
	H(6)	19.7	26.1	24.0	6.8	7.4
	H(8)	19.3	25.3	23.3	7.5	7.7
	H(9)	19.7	25.8	23.7	7.1	7.3
	H(17)	22.4	24.9	24.0	6.8	6.8
	H(18)	22.8	25.1	24.3	6.5	6.7
	H(19)	22.1	24.7	23.9	6.9	7.1
	H(20)	22.2	25.5	24.4	6.4	6.6
	H(21)	22.8	25.3	24.5	6.3	6.5
	H(22)	23.1	24.8	24.2	6.6	6.7
7[b]	H(2)	20.6	26.3	24.4	6.4	−
	H(17)	23.4	24.7	24.3	6.5	−
	H(18)	23.4	25.3	24.7	6.1	−
8[c]	H(2)	−	−	24.8	6.0	−
	H(17)	−	−	24.5	6.3	−
	H(18)	−	−	24.8	6.0	−

[a] See Scheme 2. [b] Planar **7** is the transition state for bowl-to-bowl interconversion of **8** (see Computational Section and text). [c] For bowl-shaped **8** only σ_{av} was calculated.

these two criteria.[25] This apparent anomaly has been interpreted by a computational analysis, which found that, whereas the relative stability order (ΔE_{tot}) of **3**−**5** is dominated by σ-strain imposed on the pyrene skeleton by the dicyclopenta fusion, these isomers possess nearly identical π-electron delocalisation energies (see refs.[18,19] for details). Hence, the isomers **3**−**5** represent examples of nonalternant CP-PAH in which the most stable representative need not be the most aromatic according to the magnetic criteria.[25,26]

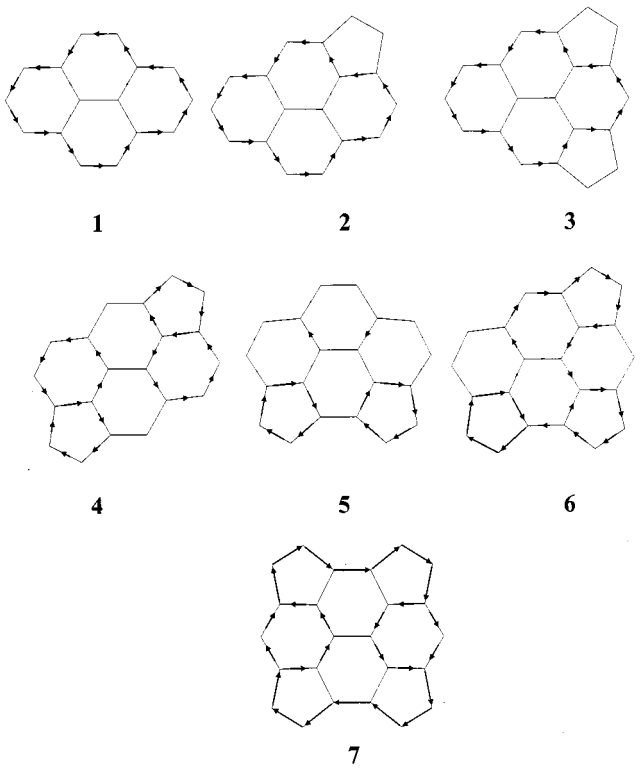

Figure 4. Schematic Hückel−London π-current density maps in planar **1**−**7**

Conclusions

Computed π- and total (σ+π)-current density maps of a family of pyrene (**1**) and its externally cyclopenta-fused congeners **2**−**8** using an ab initio distributed-origin coupled Hartree−Fock method show that the number and distribution of pentagons strongly affects the local patterns of induced currents, and that global aromaticity is reduced as more pentagons are added.

The cyclopenta moieties in **2** and **3** possess localised cyclopenteno double bonds,[18,19] and have only minor effects on the diatropic ring current of the 14π-pyrene perimeter core. For all other species **4**−**8**, intense paratropic currents in the pentagons result in stepwise destruction of the diatropic 14π-pyrene perimeter motif, resulting in the breaking up of the currents into single-ring contributions. Visualisation of the current density maps has added detail to the interpretation of Nucleus-Independent Chemical Shift (NICS) values. In fact, with the exception of compounds **6** and **7**, the main features of the pattern of paratropic contributions are explained by simple Hückel−London π-electron theory.

Computational Section

The magnetic properties of **1**−**8** were computed by using the CTOCD distributed-origin method at the ab initio coupled Hartree−Fock level of theory. In line with our previous work,[7,8] the maps were computed by using the DZ (diamagnetic zero) formulation and the integrated properties using the PZ2 (paramagnetic zero) variant, all with the

6-31G** basis using the Exeter version of SYSMO.[27] The molecular geometries were optimised at the RHF level in the 6-31G basis (RHF/6-31G)[19] using the GAMESS-UK program.[28] The optimised geometries of **1**−**8** at the RHF/6-31G, RHF/6-31G* and B3LYP/6-31G* levels of theory are practically identical and details of the energetics, such as the isomer stability order for **3**−**5**, as well as the height of the inversion barrier for **7**−**8**, are similarly insensitive to the choice of basis and level {6-31G**//RHF/6-31G total energies: −611.7857 (**1**), −687.5025 (**2**), −763.2090 (**3**), −763.2136 (**4**), −763.2167 (**5**), −838.9168 (**6**), −914.6119 (**7**) and −914.6179 a.u. (**8**) [ΔE_{tot}(**5** < **4** < **3**) = 0.0 < 1.9 < 4.3 kcal mol^{-1} and ΔE(**8** → **7**) = 3.8 kcal mol^{-1}]}.[18,19] All compounds have computed planar ground states except for tetracyclopenta[*cd*,*fg*,*jk*,*mn*] pyrene, the ground state of which is bowl-shaped with C_{2v} symmetry. This molecule also has a D_{2h} planar geometry corresponding to the transition state (one imaginary frequency) for bowl-to-bowl inversion. Compound **7** refers to the planar geometry of tetracyclopenta[*cd*,*fg*,*jk*,*mn*]pyrene and **8** to the nonplanar, bowl-shaped global minimum. Scheme 2 shows a generalised carbon atom numbering Scheme and local ring identification Scheme for **1** and its cyclopenta-fused congeners **2**−**8**.

Acknowledgments

We gratefully acknowledge travel grants from the Council for Chemical Sciences of the Netherlands Organisation for Scientific Research (CW-NWO; L. W. J.), the British Council (P. W. F. and E. S.), the Royal Society of Chemistry (International Author Travel Grant 0012289; L. W. J.), and the European Union TMR, contract FMRX-CT097−0192 (BIOFULLERENES, R. W. A. H.).

[1] [1a] U. Fleischer, W. Kutzelnigg, P. Lazzeretti, V. Mühlenkamp, *J. Am. Chem. Soc.* **1994**, *116*, 5298−5306 and references cited therein. [1b] P. von R. Schleyer, H. Jiao, *Pure Appl. Chem.* **1996**, *68*, 209−218 and references cited therein. [1c] H. J. Dauben, J. D. Wilson, J. L. Laity, *Diamagnetic Susceptibility Exaltation as a Criterion of Aromaticity*: in *Nonbenzenoid Aromatics*, vol. II (Ed.: J. P. Snyder), Academic Press, New York, **1971**, pp. 167−207 and references cited therein.

[2] P. W. Fowler, E. Steiner, A. Acocella, L. W. Jenneskens, R. W. A. Havenith, *J. Chem. Soc., Perkin Trans. 2* **2001**, 1058−1065.

[3] P. von R. Schleyer, C. Maerker, A. Dransfeld, H. Jiao, N. J. R. van Eikema Hommes, *J. Am. Chem. Soc.* **1996**, *118*, 6317−6318.

[4] For examples: P. von R. Schleyer, H. Jiao, N. J. R. van Eikema Hommes, V. Malkin, O. L. Malkina, *J. Am. Chem. Soc.* **1997**, *119*, 12669−12670. P. von R. Schleyer, B. Kiran, D. V. Simon, T. S. Sorensen, *J. Am. Chem. Soc.* **2000**, *122*, 510−513.

[5] For example: T. K. Zywietz, H. Jiao, P. von R. Schleyer, A. de Meijere, *J. Org. Chem.* **1998**, *63*, 3417−3422.

[6] T. A. Keith, R. F. W. Bader, *Chem. Phys. Lett.* **1993**, *210*, 223−231. T. A. Keith, R. F. W. Bader, *J. Chem. Phys.* **1993**, *99*, 3669−3682. R. Zanasi, P. Lazzeretti, M. Malagoli, F. Piccinini, *J. Chem. Phys.* **1995**, *102*, 7150−7157. R. Zanasi, *J. Chem. Phys.* **1996**, *105*, 1460−1469.

[7] [7a] For examples: E. Steiner, P. W. Fowler, *Int. J. Quant. Chem.* **1996**, *60*, 609−616. [7b] P. W. Fowler, E. Steiner, B. Cadioli, R. Zanasi, *J. Phys. Chem. A* **1998**, *102*, 7297−7302.

[8] [8a] P. W. Fowler, E. Steiner, L. W. Jenneskens, *Angew. Chem.* **2001**, *113*, 375−379; *Angew. Chem. Int. Ed.* **2001**, *40*, 362−366. [8b] P. W. Fowler, E. Steiner, L. W. Jenneskens, A. Acocella, *Chem. Commun.* **2001**, 659−660.

[9] For a review: R. Benshafruth, E. Shabtai, M. Rabinovitz, L. T. Scott, *Eur. J. Org. Chem.* **2000**, 1091−1106 and references cited therein.

[10] C. Tintel, J. Cornelisse, J. Lugtenburg, *Recl. Trav. Chim. Pays-Bas* **1983**, *102*, 14−20 and references cited therein. A. W. H. Jans, C. Tintel, J. Cornelisse, J. Lugtenburg, *Magn. Reson. Chem.* **1986**, *24*, 101−104. M. Sarobe, J. W. Zwikker, J. D. Snoeijer, U. E. Wiersum, L. W. Jenneskens, *J. Chem. Soc., Chem. Commun.* **1994**, 89−90 and references cited therein. See also Supporting Information of: P. I. Dosa, A. Schleifenbaum, K. P. C. Vollhardt, *Org. Lett.* **2001**, *3*, 1017−1020 and references cited therein.

[11] M. Sarobe, S. Flink, L. W. Jenneskens, B. L. A. van Poecke, J. W. Zwikker, *J. Chem. Soc., Chem. Commun.* **1995**, 2415−2416. L. T. Scott, A. Necula, *J. Org. Chem.* **1996**, *61*, 386−388.

[12] M. Sarobe, R. W. A. Havenith, L. W. Jenneskens, *Chem. Commun.* **1999**, 1021−1022.

[13] M. Sarobe, PhD Thesis, *Polycyclic Aromatic Hydrocarbons under High Temperature Conditions. Consequences for Carbon Build up during Combustion and Fullerene Formation Processes*, Utrecht University, Utrecht, The Netherlands, **1998**.

[14] For a review see: U. E. Wiersum, L. W. Jenneskens, in *Gas Phase Reactions in Organic Synthesis* (Ed.: Y. Vallée), Gordon and Breach Science Publishers, Amsterdam, The Netherlands, **1997**, pp. 143−194 and references cited therein.

[15] See for example: G. J. Bodwell, J. N. Bridson, T. J. Houghton, J. W. J. Jason, M. R. Mannion, *Chem. Eur. J.* **1999**, *5*, 1823−1827.

[16] C. Gooijer, I. Kozin, N. H. Velthorst, M. Sarobe, L. W. Jenneskens, E. J. Vlietstra, *Spectrochim. Acta, Part A* **1998**, *54*, 1443−1449 and references cited therein.

[17] Pyrene (**1**): ^{1}H NMR (300 MHz, $CDCl_3$): δ = 8.05 (2 H), 8.11 (4 H) and 8.22 (4 H). See also: L. Rodenburg, M. Floor, A. Lefeber, J. Cornelisse, J. Lugtenburg, *Recl. Trav. Chim. Pays-Bas* **1988**, *107*, 1−8.

[18] R. W. A. Havenith, H. Jiao, L. W. Jenneskens, J. H. van Lenthe, P. von R. Schleyer, M. Kataoka, A. Necula, L.T. Scott, *J. Am. Chem. Soc.*, in press and references cited therein.

[19] R. W. A. Havenith, J. H. van Lenthe, F. Dijkstra, L. W. Jenneskens, *J. Phys. Chem. A* **2001**, *105*, 3838−3845 and references cited therein.

[20] E. Clar, *Polycyclic Hydrocarbons*, Academic Press Inc., London, **1964**.

[21] J. C. Hanson, C. E. Nordman, *Acta Crystallogr., Sect. B* **1976**, *32*, 1147−1153.

[22] C.A. Coulson, R. B. Mallion, *J. Am. Chem. Soc.* **1967**, *98*, 592−598.

[23] A. Pasquarello, M. Schlüter, R. C. Haddon, *Phys. Rev. A* **1993**, *47*, 1783−1789.

[24] A. Ceulemans, L.F. Chibotaru, P. W. Fowler, *Phys. Rev. Lett.* **1998**, *80*, 1861−1864.

[25] See also: G. Subramanian, P. von R. Schleyer, H. Jiao, *Angew. Chem.* **1996**, *108*, 2824−2827; *Angew. Chem. Int. Ed. Engl.* **1996**, *35*, 2638−2641.

[26] For a special issue of *Chem. Rev.* fully dedicated to the issue of aromaticity; *Chem. Rev.* **2001**, *101*, issue 5.

[27] P. Lazzeretti, R. Zanasi, *SYSMO package (University of Modena)*, **1980**., For additional routines for the evaluation and plotting of the current density cf.: E. Steiner, P.W. Fowler, Univ. of Exeter, unpublished results.

[28] M. F. Guest, J. H. van Lenthe, J. Kendrick, K. Schöffel, P. Sherwood, R. J. Harrison, *GAMESS-UK, a package of* ab initio *programs*, **2000**. With contributions from: R.D. Amos, R.J. Buenker, M. Dupuis, N. C. Handy, I. Hillier, P. J. Knowles, V. Bonacic-Koutecky, W. von Niessen, V. R. Saunders, A. J. Stone. Derived from the original GAMESS code by: M. Dupuis, D. Spangler, J. Wendolowski, *NRCC Software Catalog*, vol. 1, program no. QG01 (GAMESS), **1980**.

Received July 2, 2001
[O01331]